Emergent Materials (2024) 7:1531–1544
https://doi.org/10.1007/s42247-024-00728-8

ORIGINAL ARTICLE

Zinc oxide nanoparticles immobilized on polymeric porous matrix for water remediation

Abdullah M. Asiri[1] · Valerio Pugliese[2] · Gerardo Coppola[2] · Sher Bahadar Khan[1] · Khalid Ahmad Alamry[1] · Soliman Y. Alfifi[1] · Hadi M. Marwani[1] · Maha M. Alotaibi[1] · Francesco Petrosino[2] · Sudip Chakraborty[2]

Received: 10 November 2023 / Accepted: 24 April 2024 / Published online: 22 May 2024

Abstract

This work proposes a novel approach to producing composite membranes by immobilizing and blending ZnO nanoparticles within a polymer matrix. The focus is investigating how different immobilization techniques impact membrane performance in critical technological applications, including membrane fouling mitigation and photocatalytic degradation. Lab-synthesized ZnO nanostructures were immobilized within a natural cellulose acetate (CA) matrix using a spray coating technique. To ensure comprehensive exploration, CA membranes with 12% and 15% wt polymer concentrations, which demonstrated superior overall performance in previous studies, were cast and prepared. The membranes underwent phase inversion, and a specially prepared ZnO solution was sprayed onto the membrane surface, creating a unique blend of polymer and nanoparticles. This comparative study highlights distinctions between nanomaterial immobilization techniques (mixing and spray coating) while maintaining identical polymer content. Such insights are crucial for both industrial applications and laboratory-scale research. The photocatalytic degradation of the reactive and toxic dye methylene blue (MB) served as a model reaction, employing a UV light module. Results unequivocally demonstrated that, irrespective of the immobilization technique employed, the combination of CA and ZnO nanoparticles significantly enhanced the photocatalytic activity of the membrane in degrading methylene blue (MB). Specifically, the dye concentration decreased from 25 to approximately 8 mg/L for both the spray coating and bulk immobilization methods, resulting in 62% and 69% dye degradation, respectively. These findings underscore the versatility of different immobilization techniques in various aspects of membrane technology. The CA-ZnO composite exhibited efficacy in photocatalytic MB degradation tests, offering promising alternatives for designing polymeric membranes tailored for contaminant removal, particularly in treating textile dye-contaminated aqueous solutions. The exploration of diverse immobilization techniques for nanocomposites presents an exciting avenue for optimization in different membrane technological processes.

Keywords Composite membrane · Spray coating · Textile dye · Photocatalyst · Cellulose acetate · Nanoparticle Synthesis

1 Introduction

Waste streams generated by the textile and agri-food sectors commonly contain a mixture of contaminants, including dyes, phenols, and pesticides. When these waste streams are released into water bodies, they pose considerable threats to both human health and the environment, leading to the formation of secondary pollutants and solid waste. Traditional methods of water treatment, such as membrane filtration, adsorption, and chemical treatment, often prove inadequate in fully eliminating dye contaminants. Membrane technology emerges as a promising and efficient approach to concentrate waste sources, effectively reducing the levels of harmful pollutants present in wastewater [1–3].

✉ Abdullah M. Asiri
aasiri2@kau.edu.sa

✉ Sudip Chakraborty
sudip.chakraborty@unical.it

[1] Chemistry Department, Faculty of Science, King Abdulaziz University, P. O. Box 80203, 21589 Jeddah, Saudi Arabia

[2] Department of Computer Engineering, Modeling Electronics and Systems (D.I.M.E.S.), University of Calabria, Via-P. Bucci, Cubo-42A, 87036 Rende, CS, Italy

Ultrafiltration (UF) and microfiltration (MF) membranes are commonly used for recovering and removing contaminants from surface water [4].

In contrast, nanofiltration membranes (NF) with a molecular weight cut-off (MWCO) in the 150-350 Dalton (Da) range exhibit significant capability for removing inorganic ions, making them suitable for wastewater treatments [5, 6]. The demand for membranes capable of regulating ions and transporting water molecules is high [7]. Polymeric materials play a crucial role in developing membranes for treating aqueous effluents due to their ease of use, reasonable cost, availability, energy efficiency, and simplicity in production at various scales. These membranes find predominant use in wastewater clarification, particularly in agriculture, textile, and industrial sectors, to purify water from contaminants [8, 9].

In wastewater treatments, the elimination of textile and industrial dyes is crucial due to their non-biodegradability and high resistance to environmental conditions. Methylene blue (MB), a well-known industrial waste dye, poses significant hazards, such as eye and skin irritation, hemolytic anemia, sickness, vomiting, and abdominal pain. Therefore, the removal of MB from polluted water is of paramount importance [10, 11].

Various processes, including chemical, physical, and biological methods, have been employed to remove dyes from aqueous solutions. Traditional wastewater treatments are inadequate at removing pollutants at ppm levels. Combining photocatalysts, particularly for treating organic pollutants, in the membrane matrix offers a unique method to facilitate contaminant degradation in groundwater environments [12–15]. A recent category of nanocomposites aims to overcome limitations and enhance performance by integrating multiple materials, such as impregnating inorganic nanoparticles into an organic polymer matrix. Unlike conventional polymers, nanocomposite membranes could exhibit improved properties, including greater dimensional exclusion, permeability, and surface area [16, 17].

he integration of nanoparticles into polymeric membrane matrices has gained considerable attention, especially for a variety of industrial and wastewater treatment applications. The use of photocatalytic degradation is notable for its cost-effectiveness, high system efficiency, and operational simplicity. Zinc oxide (ZnO) semiconductor nanoparticles have emerged as a preferred choice due to their remarkable efficacy in efficiently degrading organic pollutants. In the domain of waste treatment, there is a growing emphasis on advancing polymeric ultrafiltration and nanofiltration membranes with enhanced properties. Zinc oxide (ZnO) stands out as a pivotal element in this regard, known for its exceptional photocatalytic activity, cost-effectiveness, and distinctive characteristics [18, 19].

Metal-oxide semiconductors, such as titania (TiO2) and zinc oxide (ZnO), offer advantages like high photocatalytic efficiency, photosensitivity, non-toxic nature, low cost, and eco-friendliness. However, these photocatalysts have limitations as they can only be photoexcited in the ultraviolet (UV) region. Coupling semiconductors with different band gaps has improved their photocatalytic performance [20, 21]. The morphology of a photocatalyst, including its shape and size, may also affect its efficiency.

ZnO can be distributed homogeneously into the polymeric matrix, displaying stability under photochemical corrosion. It possesses exceptional characteristics such as high catalytic activity, unique chemical-physical properties, antibacterial resistance, low cost, high surface reactivity, and more destructive sorbent capacity compared to other inorganic catalysts [18, 22–24]. Many photocatalysts reported in the literature can be categorized as metal-based sulfides, oxides, nitrides, and metal-free compounds such as polymers [25].

Blending nanoparticles into the polymeric membrane matrix is receiving attention for potential low-cost applications [25, 26].For example ZnO/Zeolite composite photocatalysts demonstrated their effectiveness in degrading various dye pollutants in wastewater treatment applications, showcasing their potential for environmental remediation. Zinc oxide (ZnO) nanocomposites can enhance catalytic performance by integrating ZnO nanoparticles into composite structures with materials like graphene oxide, activated carbon, or metal oxides such as Fe3O4 and CuO [27]. These combinations generate synergistic effects, improving dye adsorption, light absorption, and photocatalytic activity.For example, a recent study explored a heterojunction involving Bentonite Clay supported Bi2O3/ZnO composite for detoxifying azo dyes under UV-A light [28].

Similarly, research demonstrated that ZnO nanoparticles blended with graphene oxide exhibited enhanced catalytic performance in degrading textile dye mixtures, highlighting their potential for wastewater treatment applications.Core-shell structured ZnO/Fe3O4 nanocomposites were found to efficiently remove multiple dye pollutants simultaneously, making them suitable for addressing complex wastewater scenarios [29].

Utilizing ZnO nanorods supported on activated carbon enhanced catalytic performance, effectively removing dye contaminants from industrial mixtures.Hierarchical ZnO/CuO nanocomposites effectively degraded dye mixtures under sunlight irradiation, offering a promising approach for efficient wastewater treatment [30].

Cellulose, amongst others, is the most abundant polymer, primarily used as a supporting material for fiber technology. It offers advantages such as biodegradability, eco-friendliness, bioabsorbability, and cost-effectiveness. Cellulose

acetate (CA), exhibiting these features, is one of the most used polymers for wastewater treatment membranes [31, 32].

This paper describes one of the initial approaches with innovative polymeric nanocomposite membranes (CA/ZnO) for textile dye treatment. It specifically focuses on comparing different nanoparticle immobilization techniques to enable full particle dispersion into the polymer matrix. Polymeric nanocomposite membranes can be categorized into blended nanocomposites, where nanoparticles disperse in the original solution before casting, and thin-film nanocomposite membranes, where particles form a layer on the membrane surface through pressure or dip-coating methods.

The current study proposes the synthesis and characterization of composite membranes in cellulose acetate. Subsequently, the best-performing membrane in terms of permeability undergoes photocatalytic degradation of methylene blue. Dimethylformamide/Dimethylacetamide (DMF/DMA) is proposed as a solvent for membrane preparation based on its polymer solubilization capacity [33, 34]. Two coating methods were tested for immobilizing ZnO nanoparticles on the membrane structure: ZnO dispersed within the initial solution (CA/ZnO composite membrane) and spray coating of ZnO solution, prepared through the Sol-Gel method, directly on the membrane surface via a pressure-controlled nozzle. Evaluating possible differences in immobilization techniques is essential. The primary objective of immobilizing nanoparticles is to bypass the expensive filtration process, indispensable for water decontamination. However, the issue of photocatalyst reusability, crucial for reducing associated costs, has not been addressed [34–38].

2 Materials and methods

Cellulose acetate (CA) with an average acetyl content of 39.7 wt% and an average molecular weight of approximately 50,000 (GPC) was sourced from Sigma Aldrich, Burlington, MA, USA, and utilized as the polymeric constituent for membrane casting and preparation. N-dimethylformamide (DMF) with a purity of 99%, also obtained from Sigma Aldrich, Burlington, MA, USA, was chosen to solubilize the polymer. The synthesis of zinc oxide nanoparticles through the sol-gel method involved materials such as sodium hydroxide (NaOH) with a purity of ≥98% (Sigma Aldrich), ethanol (CH_2COOH) from Humbug Chemicals, and zinc acetate dihydrate ($Zn(CH_3COOH)2.2H_2O$) with a purity of ≥99% from Humbug Chemicals.

Zinc acetate dihydrate served as the primary precursor for synthesis, with ethyl alcohol as a reagent and distilled water as the solvent. A Glycerol solution from Honeywell, Morristown, NJ, USA, was employed in membrane-washing operations. Local manufacturers supplied Methylene Blue for everyday applications. The main components of the UV source light were derived from a mechanical solar simulator model no. 21117 (Newport, CA, USA). Permeate flux was assessed using the following:

$$J = \frac{V}{(A \times t)} \tag{1}$$

where J is the permeate flux (L/m^2h), V is the volume of the accumulated permeate, and A is the membrane surface area and the filtration time. The effective passage surface of the membrane is 12.68 cm^2. For operation in constant flow mode, a gas pump was connected to the inlet of the Millipore filtration cell and conveyed the permeated solution from the outlet. Three different transmembrane pressures were analyzed for each experiment, and each experiment was conducted at least in triplicate. The rejection, R, is calculated using the following equation:

$$R = 1 - \frac{C_P}{C_F} \tag{2}$$

where CP is the permeate concentration and CF is the feed concentration.

2.1 ZnO nanostructures synthesis

ZnO nanoparticle solution has been prepared through the sol-gel technique. The preparation requires sodium hydroxide (8 grams) and zinc acetate dihydrate (2grams). Subsequently, the component's solubilization occurs in different volumes of distilled water under agitation for 5-6 minutes hydroxide in 10 ml and zinc acetate dihydrate in 15 ml. Shortly after, the solutions were mixed for about 15 minutes under continuous agitation by pouring the sodium hydroxide mixture into the zinc acetate; the resulting solution was titrated by dropping 100 ml of ethyl alcohol. The agitation leads to a transparent alabaster residue on the bottom of the graduated glass tube, thus indicating that the process occurred correctly. The entire hydrolytic reaction of zinc acetate assisted by NaOH in an ethyl alcohol solution leads to the formation of a ZnO-based solution generated by the balance betwixt the addition/hydrolysis and the dehydration/condensation reactions. Since a high temperature occurs, acetate and zinc ions formation occurs due to the hydrolytic reaction that involves zinc acetate. The electrons inside the oxygen molecules allow the anchorage between the zinc ions and the functional/hydroxyl-OH moieties of the ethyl alcohol particles. The overall chemical reaction to form ZnO Nano-powder follows Eq. (3):

$$\left(Zn\left(CH_3COO\right)_2 \cdot 22H_2O\right) + 2NaOH \rightarrow ZnO + 2Na\left(CH_3COO\right) + 2H_2O \tag{3}$$

2.2 Preparation of photocatalytic cellulose acetate membranes

Two methods were attempted for immobilizing ZnO nanoparticles on the membranes: immobilization into the feed solution and spray coating. Before spray coating, the ZnO solution was dispersed in distilled water (0,1% w/v) and used as the coating suspension. The apparatus for spray coating using ZnO sol-gel consists of a nozzle connected to a pressure source (0.5 bar) that draws from a module containing the nanoparticle solution.

A sprayer is fixed at a constant distance from the membrane at a pressure of 0.8 bar. The membranes were placed horizontally on glass and sprayed continuously from a distance of 10 cm for 10 to 40 seconds. Then, they were dried for one day in an open container permitting. This way, the contact between the solution and the membrane occurred.

2.3 Composite membrane preparation

The methodology involved the dissolution of cellulose acetate (CA) in N-dimethylformamide (DMF) to form a polymer solution. The solution underwent stirring at 75 °C in a water bath for 3-4 hours, leading to the fabrication of cellulose membranes through the phase inversion method. To enhance the membrane properties, various amounts of ZnO were introduced into the polymeric solution, and the ZnO quantity was optimized for the most effective membrane composition.

Subsequently, the polymeric solutions were left unstirred at 60 °C for eight hours to facilitate the removal of air bubbles. This was followed by a 12-hour period in a fume hood to eliminate additional air bubbles in a vacuum environment. To prevent solution aggregation, the mixture was then stored in an ultrasonic bath at 60 °C for 8 hours.

The resulting flat sheet membranes exhibited a skin layer thickness of approximately 150 µm [18]. Post-precipitation, the membranes were taken out of the coagulation bath and thoroughly washed with distilled water to eliminate excess solvent. Multiple washing steps were employed to ensure the complete removal of the DMF solvent from the membrane matrix.

The obtained membranes were dried at room temperature to eliminate residual water, resulting in the formation of a porous and dry flat membrane. Finally, for preservation and future use, the dried membrane was immersed in an aqueous glycerol solution (10% v/v). The composition of all suspensions was expressed as a weight percentage (wt%) of ZnO relative to the total solute mass, as outlined in Table 1.

An ultrasound bath operation was utilized to achieve an excellent dispersion of ZnO particles, following procedures described in previously published works [33, 33]. The membrane preparation process was guided by references to those obtained in prior articles. Notably, zinc oxide in CA-Z1 membranes underwent bulk immobilization, serving solely as benchmarks in specific analyses to ensure experimental control and comparison.

2.4 Experimental setup and design

The experimental procedures were meticulously developed and executed within the laboratory confines.

The process began with the preparation of polymeric membranes through the phase inversion method. Subsequently, these membranes underwent a carefully designed spray coating process to ensure the uniform application of nanoparticle solutions onto the upper region of the membrane pores. To facilitate the spraying of the pre-prepared ZnO suspension, the module nozzle was securely connected to a compressed air system with a consistent pressure of approximately 0.8 bar. Key parameters employed during the spray coating process are comprehensively outlined in Table 1. Following the spray coating, the samples underwent a natural drying period lasting 7 h. This was succeeded by heating in an oven, starting from room temperature and gradually reaching 100 °C at a controlled rate of 0.5 °C per minute. The samples were soaked for 1 h at this temperature and then subjected to further heating at a rate of 3 °C per minute to the target temperature, where they were soaked for a specific duration. All pertinent parameters involved in the spray coating process are succinctly summarized in Table 2. Post-treatment, crucial for eliminating excess solution on the membrane surface, the flat sheets were carefully positioned inside the Millipore module. To assess their degradation resistance, the membranes were exposed to a UV lamp. Specifically, artificial UV lamps emitting UV-A rays ($\lambda = 355–365$ nm) were chosen as light sources. This strategic selection enabled ZnO, a semiconductor, to catalyze

Table 1 Membrane preparation [1]

Cellulose	(%)	ZnO (%)	DMF (%)	Cellulose (g)	DMF (g)	ZnO (g)
CA12-SP	12	0	88	2.4	17.6	0
CA12-Z1	12	1	87	2.4	17.4	0.2
CA15-SP	15	0	85	3	17	0
CA15-Z1	15	1	84	3	16.8	0.2

Table 2 Spray coating parameters

Spray Parameters	Pressure [Bar]	Distance [cm]	Flow rate[g s^{-1}]	Spray Time [s]	Dry Time [hr]
Values	0,8	60	0,5	10–40	7

advanced oxidation reactions, thereby facilitating the degradation of Methylene Blue (MB) present in the water. For enhanced clarity, Fig. 1 provides a schematic representation of the entire experimental process.

2.5 Membrane characterization

Characterization techniques play a crucial role in understanding the membrane structure and its chemical properties, providing valuable information for optimizing membrane performance. Various methodologies were employed to investigate the chemical and physical characteristics of the membranes, including x-ray diffraction (XRD), scanning electron microscopy (SEM), and contact angle measurements. Additionally, a UV spectrophotometer was utilized to analyze the UV-vis absorption spectrum for the identification of synthesized ZnO.

1. X-Ray Diffraction (XRD):
   - XRD analysis was conducted using Bruker equipment (D8 ADVANCE) with a monochromatic Cu Kα (λ = 0.154 nm) radiation source.
   - The analysis operated at 40 mA and 40 kV between 20° and 70° to confirm the presence of ZnO nanoparticles in the membrane.
2. Scanning Electron Microscopy (SEM):
   - A SEM microscope (Thermo Fisher Phenom Pure G6) was used to investigate both the membrane surface morphology and cross-section.
   - Membrane samples were subjected to freezing in liquid nitrogen to maintain the unaltered film structure.
   - The cracked membrane samples were loaded into the sample holder for SEM investigation, and various images were processed and presented in the results section.
3. Water Contact Angle Measurements:
   - The hydrophilicity of the membrane surface was assessed through water contact angle measurements using the tensile drop method on a contact angle meter (KSV Instruments LTD, Helsinki, Finland).
   - A minimum of four measurements were taken by depositing a 5 µL ultrapure water drop on the membrane at ambient temperature.
4. UV Spectrophotometer Analysis:
   - A UV spectrophotometer was employed to analyze the UV–vis absorption spectrum for the identification of synthesized ZnO.

These characterization techniques collectively contribute to a comprehensive understanding of the membrane's structure, morphology, and chemical properties. The information derived from these analyses can be instrumental in optimizing the membrane design and composition to enhance overall performance.

2.6 Catalytic degradation of MB

The photocatalytic analysis of the prepared membrane has been performed. The methylene blue (MB) degradation rate under UV irradiation was measured. A Millipore membrane module was inserted into a UV irradiation case where a mechanical solar simulator (model no. 21117, Newport, USA) was used to irradiate the membrane module during the UF experiment, as explained in Fig. 1. During the degradation experiment, samples were collected regularly from the permeate stream and investigated into the spectrophotometer.

Before the photocatalytic reaction, MB's feed solution was continuously recirculated through the membrane module in the dark phase without UV to guarantee any possible adsorption of MB on the membrane pores. Monitoring of

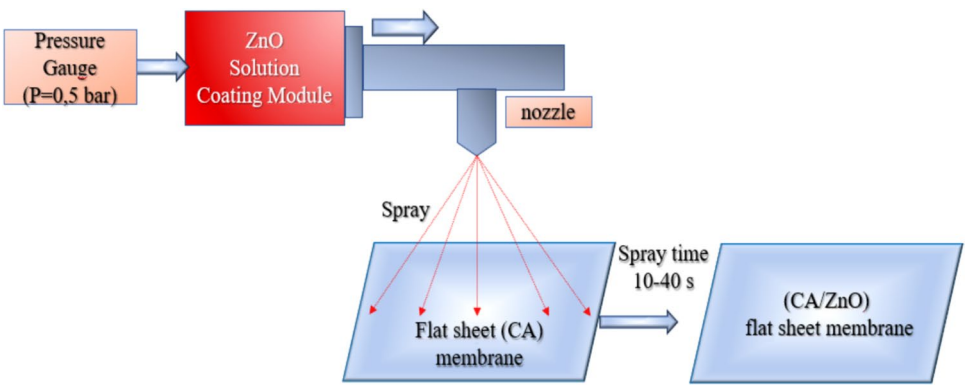

Fig. 1 Experimental process schematic

permeate concentration was performed until a steady state flux was observed. Then, a solar simulator was switched on so that the UV could activate the membrane and the ZnO surface. The used wavelengths in the photocatalytic reactor were chosen in the 315–400 nm range. UV light distance from the membrane is about 10 cm from the surface side.

2.7 Characterization of permeate product

UV–vis spectrophotometry at 664 nm measured the feed and permeated MB concentration. Quantitative analysis of the components contained in the permeate solution was made using HPLC (Thermo Scientific Dione Ultimate 3000 Photodiode Array Detector), to check the MB concentration measured by spectrophotometry. A C18 Reversed-phase LC column (Acclaim-120) working at 25 °C was used. 10 µL was the injection volume inside the column, whereas the eluent flow rate was 0.2 mL/min. The permeate concentration in HPLC was measured from the peak as obtained in the chromatogram. Distinct peaks attributed to the degradation products and non-degraded MB from the chromatographic graph.

3 Result and discussion

3.1 Membrane characterization: microscopic analysis of membrane surfaces

3.1.1 SEM investigations

SEM analyses were conducted to scrutinize the impact of different immobilization techniques on the morphological properties of asymmetric membranes. The figure presented provides a comprehensive insight into the SEM investigation performed on a CA15-Z1 membrane after the ZnO spray coating procedure. This optical examination yields crucial information regarding membrane characterization, morphology, porosity, and the effectiveness of catalyst entrapment on the membrane surface. Similar to membranes featuring bulk-immobilized ZnO, the spray-coated samples exhibit the formation of a skin layer, prompting rapid demixing between the solvent and non-solvent during the phase inversion process. This observed phenomenon underscores the significance of the spray coating technique in influencing the structural characteristics of the membrane. Understanding such effects contributes valuable knowledge to the immobilization process, enhancing our comprehension of its implications for membrane performance (Fig. 2).

The sample's large-scale topology reveals a smooth and homogeneous surface (Fig. 3a), with sparse micropores (300 to 800 nm radius) resulting from the hand-driven casting methodology. The cross-section (sector b) shows a uniform sponge layer with a depth of 30±6 mm. In a cut section (sector c), a dense outer layer of 2-3 nm depth is observed, covering the inner sponge layer. The inner layer displays perpendicular channels with a radius of approximately 7±2 mm, visible in the cross-section (sector d). A clearer cross-section view (sector e) reveals cavities and nanopores in the inner sponge layer, with pore radii ranging from 140 to 220 nm. Catalyst deposition on the membrane surface through spray coating is evident in a scan of the outer layer (section f), showing catalyst particles with diagonals within the range of 7±2 mm.

Membranes functionalized with ZnO dispersed directly into the mass exhibit asymmetry in the cross-sectional configuration, featuring a fine selective layer and porous finger-like and spongy structures in the lower sublayer. The skin layer forms due to immediate demixing between solvent and non-solvent during the phase inversion process, driven by the elevated mutual diffusivity of water and DMF. Functionalization of ZnO in bulk increases the number of pores (lower formation of macro-voids) due to the higher diffusion rate of the solvent phase (water) compared to the solvent (DMF). This difference affects both thermodynamics and kinetics, leading to a slight increase in the suspension viscosity.

Comparing the tested membranes, it is evident that bulk functionalization results in a more uniform distribution of ZnO particles throughout the membrane compared to the spray coating process (Fig. 4h, g).

3.2 Membrane characterization: contact angle, permeability, and rejection rate measurements

Table 3 collects water contact angle and permeability values for CA membranes mixed with ZnO by bulk immobilization and spray coating. The water contact angle is one of the most effective methods for evaluating the surface hydrophilicity of membranes. The more the surface hydrophilicity of the membrane increases, the more its contact angle decreases at contact angles of less than 90°. In particular, as reported in the literature, due to the contribution of ZnO structures, composite nanoparticle membrane exhibits improved hydrophilicity compared to pure polymeric membranes. The more significant hydrophilic tendency can be attributed to the ability of ZnO nanoparticles embedded in the membrane surface to form hydrogen bonds with water molecules, which increases the water adsorption capacity and improves membrane hydrophilicity [33, 39]. CA12 membranes have similar and comparable contact angle values, which implies a similar mechanism in the arrangement of zinc oxide on the membrane surface.

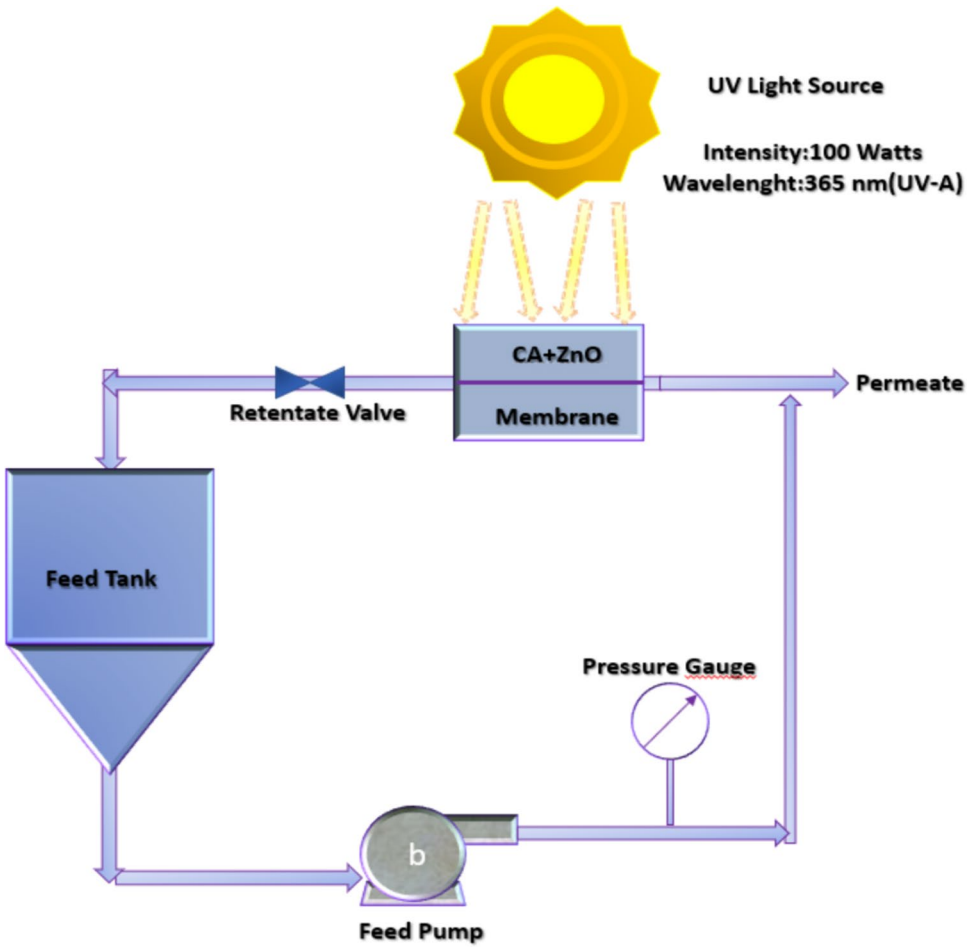

Fig. 2 Photocatalytic membrane (CA-ZnO) system/reactor

The results show that the contact angle is smaller for samples prepared with ZnO in solution than spray-coated ones. This tendency could be attributed to lower efficiency in the spraying process, resulting in non-uniform distribution of the solution within the membrane's pores. No appreciable flow value was detected for CA15 membranes that immobilized bulk and spray-coated. These virtually zero permeability values are attributable to several CA clusters that form an extremely thick membrane layer (up to 150 µm), making it non-permeable up to 5 bar pressure. In order to demonstrate the potential effects of UV rays on prepared membranes' permeation properties, it was decided to calculate the rejection rate before and after the photocatalytic treatment.

Methylene blue rejection values of prepared membranes subjected to photocatalytic treatment reached approximately 88-89% for CA 12% wt membranes, which showed the best performance data, demonstrating the combination of polymeric membranes and laboratory-synthesized nanomaterials (ZnO) highly suitable for dye treatment. Comparing the data mentioned above, it is possible to observe that the results in photocatalytic tests are much more satisfactory in terms of the rejection rate of membranes treated without UV light, which stands at 63%. These findings underscore the importance of ZnO immobilization methods in influencing membrane properties, including hydrophilicity and permeability. Additionally, the positive impact of photocatalytic treatment on dye rejection further highlights the potential of these membranes in wastewater treatment applications.

3.3 Membrane characterization: XRD analysis of the membrane surfaces

The actual presence of ZnO nanoparticles immobilized within the spray-coated polymer matrix was verified through XRD analysis.Using XRD analysis, it is possible to observe how the ZnO particles have deposited on the surface of the membrane and, in particular, inside the membrane's pores. XRD analysis can estimate peak enlarging with crystallite size, which is evaluated by broadening a particular XRD peak in a diffraction pattern. The diffraction pattern is associated with a characteristic planar reflection within the crystal unit cell. These diffractograms contribute to the understanding of the structural characteristics of the ZnO deposit on the CA membranes, providing valuable information about crystal orientation, size, and potential variations in crystal structure.

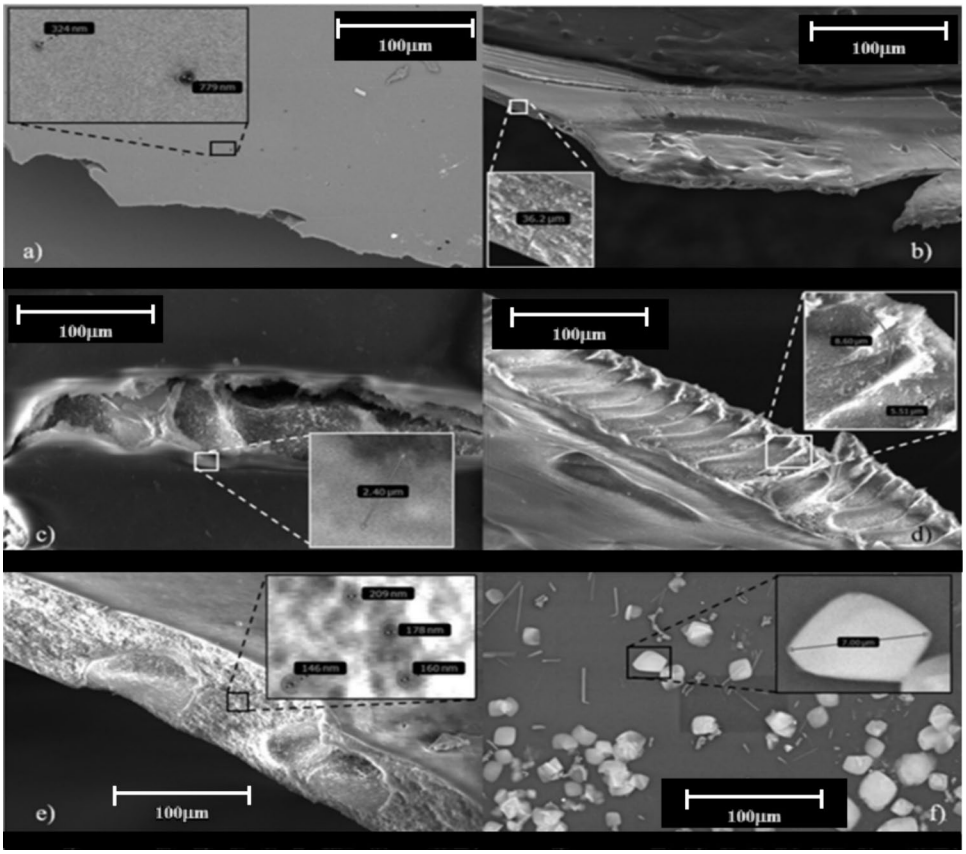

Fig. 3 SEM images of a CA15-Z1 sample: **a** outer layer topology, **b** cross-section scan, **c** inner layers through a superficial sample cut, cross-section features: **d** channeling and (**e**) sponge layer magnification, **f** catalyst deposition

Figure 5 shows the diffractograms of CA spray-coated with ZnO nanoparticle solution referring to the CA membrane of 12% by weight and 15% by weight, respectively. In addition, well-defined and pointed peaks demonstrate how the ZnO deposit formed is effectively present on the membrane's surface. The ZnO diffractogram for both membranes exhibited similar dominant peaks at 2θ angles of 36° and 37°, which correspond to the prominent characteristic peaks of zinc-oxide nanoparticles.

Both CA 's composite membranes also showed different peaks of ZnO nanoparticles at 43° and 42°. The film deposited after the spray coating for both CA 12, 15% wt presents a polycrystalline structure with a (peak 37° circa) preferred orientation. Both membranes show secondary peaks for similar angle values (16°;17°), (25°; 27°); the crystallites undergo a preferred orientation with a decrease of peak intensity. The width of the peaks, inversely proportional to the crystal size, is extraordinarily thinner, corresponding to a larger crystal size. The most significant and prominent peaks may suggest the presence of smaller dimension crystals or a different crystal structure. This observation could be attributed to the new ZnO synthesis method or lower crystallinity, as evidenced by SEM analysis and confirmed by literature [40, 41].

3.4 Membrane characterization: photodegradation study

The photocatalytic degradation of methylene blue (MB) is primarily localized on the photocatalyst's surface, triggered by exposure to light with energy levels surpassing its band gap. This activation initiates the generation of electron-hole pairs, and their recombination dynamics are influenced by voids and interstitials, introducing deep-level defects within the band gap. Non-recombinant charges are consequently produced, allowing migration on the catalyst's surface and participation in redox reactions with adsorbed water, oxygen, and organic species.

Within the valence band (VB) of zinc oxide (ZnO), photogenerated holes react with water molecules, resulting in the formation of hydroxyl groups (OH^-) or hydroxyl radicals (OH•). Simultaneously, photogenerated electrons in the ZnO conduction band (CB) react with oxygen molecules, generating superoxide radicals (O_2•). These radicals play a pivotal role in the degradation of methylene blue. The degradation pathways involve direct reactions with VB holes and non-direct reactions facilitated by non-selective OH• oxidizing radicals, ultimately leading to the mineralization of MB molecules into non-toxic compounds, such as radicals.

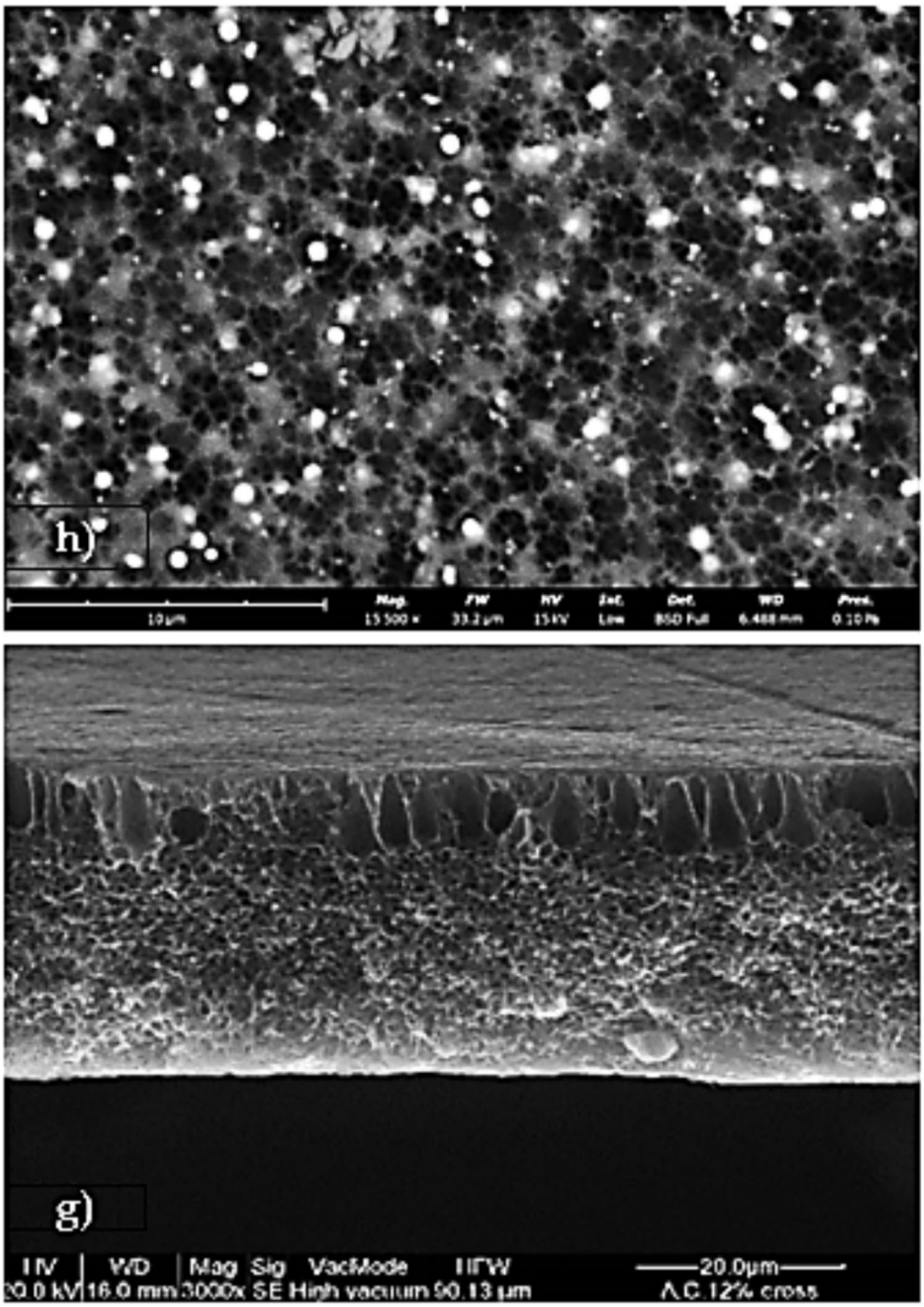

Fig. 4 Surface SEM images of membrane with ZnO dispersed in solution: top view of the asymmetric CA membrane 12% CA + ZnO (**h**),cross-section of the asymmetric CA membrane 12% CA + ZnO(**g**)

Table 3 Water contact angle of the prepared membranes

Membrane Code	Permeability (LMH/bar)	Contact Angle
CA12-SP	410	80.2 ± 0.6
CA12-Z1	439	77.1 ± 2.3
CA15-SP	0	81.7 ± 1.9
CA15-Z1	0	76.0 ± 2.3

The composite membrane, comprising cellulose acetate (CA) and ZnO, underwent UV irradiation (365 nm, 100 W) for 45 minutes in the presence of MB, highlighting ZnO's effectiveness in decomposing the dye in water.

During UV-light irradiation of the ZnO-loaded composite membrane, photogenerated electron-hole pairs react with O_2 and H_2O on the ZnO surface, forming O_2^- and OH^-, contributing to MB degradation. The degradation rate for the CA 12% wt membrane stabilizes after 10 minutes. However, a comparative analysis in Fig. 5 illustrates differing

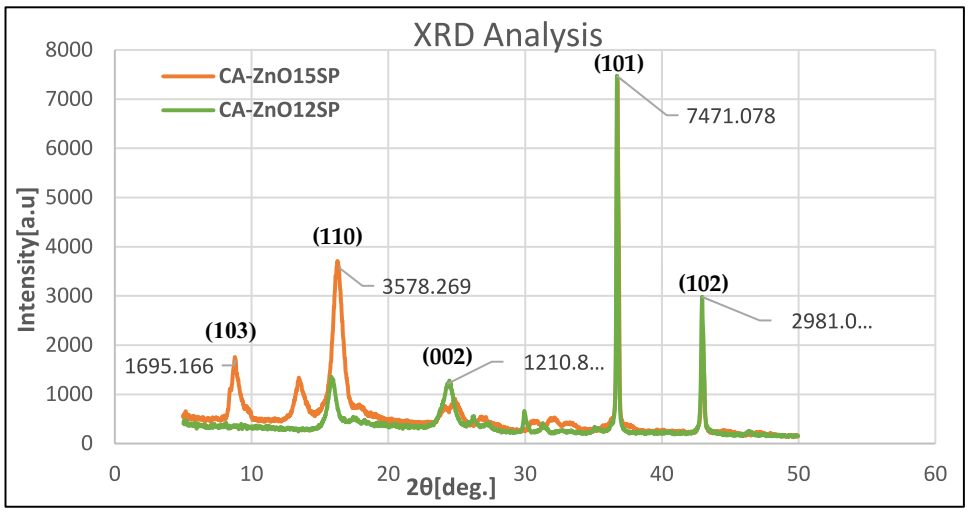

Fig. 5 XRD analysis and patterns of CA- ZnO spray coated membranes

degradation tendencies between the spray-coated CA 12% and 15% membranes. The CA 12% wt membrane exhibits a notably quicker degradation rate, reaching equilibrium in approximately 5-10 minutes. This phenomenon is attributed to limited active site availability, causing repulsion between dye particles and the catalyst surface, resulting in a decline in the degradation rate.

Efficiency in dye degradation diminishes with an increasing initial concentration due to the adsorption of excess dye molecules on the catalyst surface, reducing the availability of active sites. The comprehensive dataset collected facilitates a nuanced understanding of the degrading effect on the MB feed solution.

Starting from data of MB concentration in time is possible to evaluate Degradation efficiency throuught the equation (4):

$$Degradation\ Efficiency\ \% = \frac{C_o - C_{(t)}}{C_0} \times 100 \quad (4)$$

Where Co is the MB feed concentration, $C_{(t)}$ is the MB concetration evaluated at a fixed time collected every 5 min. All the degradation efficiency result are listed in the following table (Table 4).

The degradation efficiency values are comparable to those available in the ZnO literature. The removal efficiency of ZnO nanoparticles synthesized from zinc acetate in this study is comparable to other methods employed in previous studies, as shown in Table 5. The lower % degradation values of the present work may be due to the shorter reaction time that characterized our tests. Another important parameter that can affect the photodegradation studies is pH. The efficiency of photocatalytic degradation processes, exemplified by the decomposition of Methylene Blue (MB) in aqueous solutions under UV light, is notably influenced by the pH level of the solution. Our

Table 4 Degradation efficiency (DE%) of the prepared membranes

Time[min]	CA15_R(%)	CA12SP_R(%)	CA12Z1_R(%)
5	90.6	5.6	5.7
10	76.3	19.3	22.9
15	84.5	30.3	34.3
20	80.1	35.1	43.4
25	94.4	41.3	50.2
30	94.6	48.2	55.9
35	75.6	52.1	59.8
40	97.1	57.8	63.5
45	98.8	61.9	68.0

study, conducted at a pH of 6.3, observed a degradation efficiency that fell between the highest efficiency achieved at pH 8.5 and the lowest at pH 3.5. This observation is consistent with findings in the existing literature, underscoring the importance of pH optimization in augmenting the efficacy of photocatalytic degradation processes across diverse applications [42, 43].

The membranes were tested to treat simulated polluted water with a single dye; a solution including distilled water and MB has been prepared to perform the tests.

The test was conducted by collecting the same amount (4 ml) of textile dye (MB) every 5 for a total of 45 min and was replicated several times to estimate the standard deviation and evaluate the method's repeatability. Optically, it is possible to observe the colour change of the solution subjected to UV light. This changes from the feed's dark blue colour Fig. 6 (a) to a much lighter shade of blue (b,c); this implies a reduction in the concentration of MB in the solution during the process.

The existing literature acknowledges that an elevation in methylene blue (MB) concentration necessitates a corresponding increase in the number of hydroxyl radicals

essential for its efficient degradation [49]. Figure 7 presents a comparative analysis of various immobilization techniques and their impact on membrane degradation efficacy. The focus was on analyzing cellulose acetate (CA) membranes with a 12% weight concentration, demonstrating superior catalytic performance.

The curves in Fig. 7, representing different immobilization techniques, showcase remarkably similar rates and slopes. This consistency underscores the electronic interaction between CA and ZnO, contributing to notable catalytic activity owing to the strong affinity between the polymer and nanoparticle [50]. The discerned linear trend in the graphs serves as additional confirmation that the degradation process of Methylene Blue (MB) adheres to pseudo-first-order kinetics. The significant surface area offered by the polymeric microfibers of cellulose acetate

Table 5 Methylene Blue degradation with ZnO different nanoparticles under UV light catalyst methods

Catalyst	Method	DE(%)	Operation Time(min)	Ref
Nanosized ZnO	Sol–gel	94	90	[44]
Nanosized ZnO	Precipitation	98	90	[45]
ZnO nanoparticles	Precipitation	89.2	90	[46]
ZnO nanoparticles	Sol–gel	69	200	[47]
Nitrogen doped ZnO nanoparticles	Hydrothermal method	95	40	[48]
ZnO nanoparticles	Sol–gel	61.9	45	Present Study

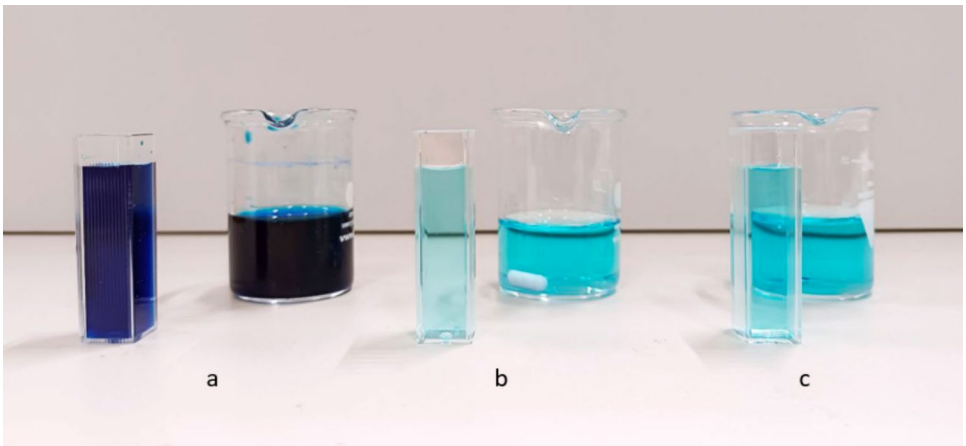

Fig. 6 Optical Comparison between dye before (**a**) and after degradation using different immboliziation techniques: (**b**) Bulk ZnO dispersion and (**c**) Spray Coating

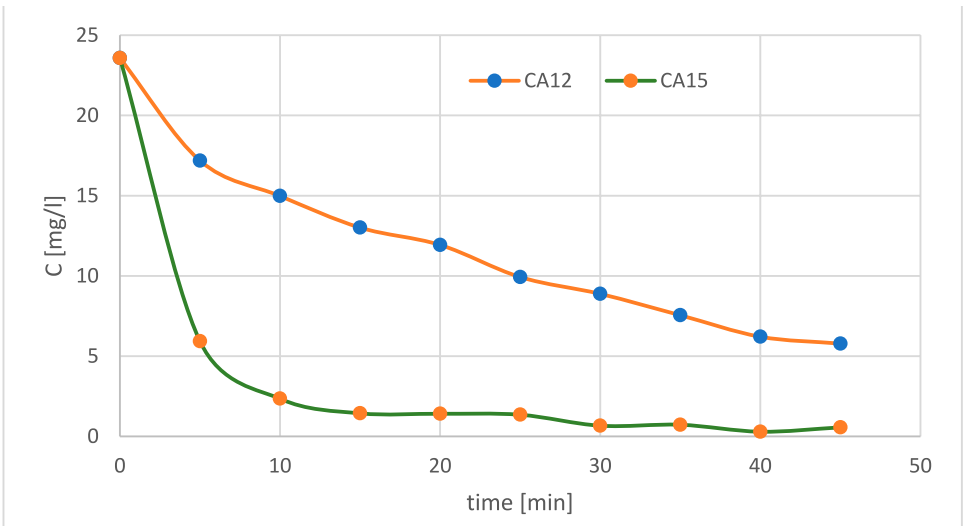

Fig. 7 MB concentration in time on CA-ZnO spray-coated membranes with 1% of ZnO and two different CA concentrations of 12% and 15%

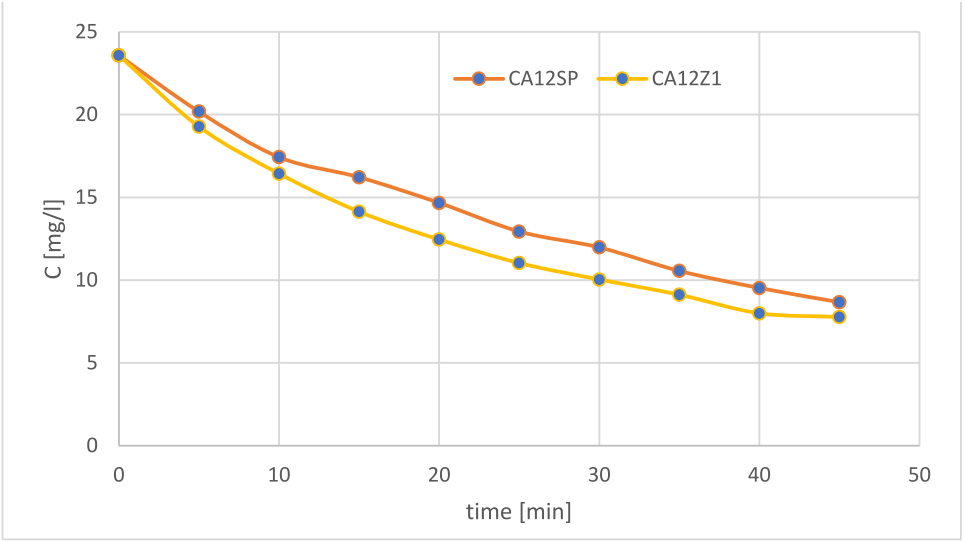

Fig. 8 MB concentration in time on CA 12% wt membranes with different ZnO Immobilization technique

is instrumental in achieving this linear behavior. The noteworthy surface-to-volume ratio of ZnO, in conjunction with exposure to UV light, amplifies the number of active sites on the membrane surface. This collaborative effect results in an outstanding level of reactivity, underscoring the pivotal role played by the unique characteristics of cellulose acetate microfibers and the favorable surface properties of ZnO in catalyzing the degradation process [51–56] (Fig. 8).

4 Conclusions

In this work, after casting and characterizing the modified cellulose acetate ZnO (CA/ZNO) membrane,a methylene blue photocatalytic degradation test was conducted employing the matrix that exhibited the best permeability values. It has been extensively demonstrated in work presented by our team that the composite membrane (acetate cellulose and zinc oxide) can degrade toxic MB with less poisonous components beneath laboratory conditions. Spray coating is an effective method that uses different characterizations performed with the composite membrane, confirming homogeneous nanocatalyst distributions on the polymer matrix of the membrane. The membranes that showed the best photodegradation values in the previous work were those prepared with 12% and 15% wt of CA. According to the previous work, the 12% CA membrane with a 0,1% ZnO membrane showed higher degradation efficiencies than the other. These membranes were prepared without ZnO in the formulation and later spray-coated with 0.1% wt ZnO solution to immobilize the nanoparticle. The results obtained in these last works have shown how the CA membrane mixed with ZnO nanoparticles can effectively work for MB or other toxic chemical degradation.

The quality of the results also bypasses the type of immobilization to which the nanoparticle is subjected. It is essential to highlight how the zinc oxide obtained through the sol-gel method is sprayed in the form of a solution directly onto the surface of the membrane and is characterized by particles with smaller average sizes. This dissimilarity in average size depends on the different processes by which zinc oxide was synthesized; with the autoclave method, heating in the oven leads the zinc oxide particles to dry out and form clusters. Some process control parameters still need to be studied, demonstrating that this technology, as mentioned above, has some limitations due to the future optimization of the spray coating process.

Acknowledgements The authors extend their appreciation to the Deputyship for Research & Innovation, Ministry of Education in Saudi Arabia for funding this research work through the project number (IFPNC-006-130-2020) and King Abdulaziz University, DSR, Jeddah, Saudi Arabia and S.C acknowledge the support of PRIMA Foundation under GA 2024 for part of the work.

Author contributions A.M.A.: Conceptualization, Editing, Funding Acquisition, V.P. and G.C: Conceptualization, Investigation, Formal Analysis, Writing Original Draft, Review & Editing, S.B.K.: Review & Editing including analysis of data. K.A.A.: Review & Editing; S.Y.A.: Writing & Editing; H.M.M.: Writing—Review & Editing; M.M.A.: Writing Review & Editing; F.P.: Formal Analysis; S.C.: overall supervision of the work, Methodology, Formal Analysis, Writing, Review & Editing, and Funding Acquisition. All authors have read and agreed to the published version of the manuscript.

Funding Open access funding provided by Università della Calabria within the CRUI-CARE Agreement. Ministry of Education in Saudi Arabia and King Abdulaziz University, DSR, Jeddah, Saudi Arabia. Also, thank MDPI for providing us with the financial support to cover the APC.

Data availability Not applicable.

Declarations

Conflicts of interest The authors declare that they have no known competing financial interest or personal relationships that could have appeared to influence the work reported in this paper.

Institutional review board statement Not applicable.

References:

1. A.M. Asiri et al., Photocatalytic Degradation of textile dye on blended cellulose acetate membranes. Polymers (Basel). **14**(3) (2022). https://doi.org/10.3390/POLYM14030636
2. Y. Zhang, S. Wei, Y. Hu, S. Sun, Membrane technology in wastewater treatment enhanced by functional nanomaterials. J. Clean. Prod. **197**, 339–348 (2018). https://doi.org/10.1016/J.JCLEPRO.2018.06.211
3. P. Muñoz, K. Pérez, A. Casino, R. Ruby-Figueroa, Recovery of anthocyanins and monosaccharides from grape marc extract by nanofiltration membranes. Molecules **26**(7), 2003–2003 (2021). https://doi.org/10.3390/MOLECULES26072003
4. N. Nasrallah, L. Halacha, V. Amanpour, A. Chateau, Photocatalytic-membrane technology: a critical review for membrane fouling mitigation. J. Ind. Eng. Chem. **93**, 101–116 (2021). https://doi.org/10.1016/J.JIEC.2020.09.031
5. A. Casino, C. Conidia, R. Ruby-Figueroa, R. Castro-Muñoz, Nanofiltration and tight ultrafiltration membranes for the recovery of polyphenols from argo-food by-products. Int. J. Mol. Sci. **19**(2) (2018). https://doi.org/10.3390/IJMS19020351
6. M. A. A. Shahrazad and A. Zargari, Nanocomposite membranes. Emerg. Technol. Sustain. Desalination Handb. 285–330 2018. https://doi.org/10.1016/B978-0-12-815818-0.00009-6
7. Y. Li, S. Wang, G. He, H. Wu, F. Pan, Z. Jiang, Facilitated transport of small molecules and ions for energy-efficient membranes. Chem. Soc. Rev. **44**(1), 103–118 (2015). https://doi.org/10.1039/C4CS00215F
8. A.J. Jose, J. Kaipen, M. Alegar, Polymeric membranes: classification, preparation, structure physiochemical, and transport mechanisms. Fundam. Biomater.: Polym. 21–35 2018. https://doi.org/10.1016/B978-0-08-102194-1.00002-5
9. S. Haidari, H. Etemadi, R. Yeganeh, A comprehensive analysis of membrane fouling in microfiltration of complex linear macromolecules based on theoretical modelling and FESEM images. J. Chem. Technol. Biotechnol. **96**(2), 360–373 (2021). https://doi.org/10.1002/JCTB.6548
10. D.A. Yaseen, M. Scholz, Textile dye wastewater characteristics and constituents of synthetic effluents: a critical review. Int. J. Environ. Sci. Technol. **16**(2), 1193–1226 (2019). https://doi.org/10.1007/S13762-018-2130-Z/TABLES/7
11. V. Katherina, J. Kaneda, S.Y. Lau, Efficiency of various recent wastewater dye removal methods: a review. J. Environ. Chem. Eng. **6**(4), 4676–4697 (2018). https://doi.org/10.1016/J.JECE.2018.06.060
12. D. Yu, Y. Wang, M. Wu, L. Zhang, L. Wang, H. Ni, Surface functionalization of cellulose with hyperbranched polyamide for efficient adsorption of organic dyes and heavy metals. J. Clean. Prod. **232**, 774–783 (2019). https://doi.org/10.1016/J.JCLEPRO.2019.06.024
13. J. Kim, B. van der Brugger, The use of nanoparticles in polymeric and ceramic membrane structures: review of manufacturing procedures and performance improvement for water treatment. Environ. Pollut. **158**(7), 2335–2349 (2010). https://doi.org/10.1016/J.ENVPOL.2010.03.024
14. P. Nonmatch, S. Chantay, R. Malachi, W.C. Oh, Noncatalytic performance of ZnO/graphene/TiO2 nanocomposite for degradation of dye pollutants (methylene blue, termite BAC-L, termite BBU-L and termite NFW-L) under ultrasonic irradiation. Dyes Pigm. **134**, 487–497 (2016). https://doi.org/10.1016/J.DYEPIG.2016.08.006
15. D. Yu, L. Li, M. Wu, J.C. Crittenden, Enhanced photocatalytic ozonation of organic pollutants using an iron-based metal-organic framework. Apple Catalo B **251**, 66–75 (2019). https://doi.org/10.1016/J.APCATB.2019.03.050
16. J. Njuguna, F. Ansari, S. Sachse, H. Zhu, V.M. Rodriguez, Nanomaterials, nanofillers, and nanocomposites: types and properties. Health Environ. Saf. Nanomater.: Polym. Nanocomposites Other Mater. Containing Nanoparticle. 3–27 (2014). https://doi.org/10.1533/9780857096678.1.3
17. N. Chandran, C. Harishchandra, S. Thomas, Rheology of polymer-clay nanocomposites. Rheology Polym. Blends Nanocomposites: Theory Model. Appl. 97–122 (2020). https://doi.org/10.1016/B978-0-12-816957-5.00006-9
18. L.Z. Pei, T. Wei, N. Lin, H.Y. Yu, Synthesis of zinc oxide and titanium dioxide composite nanorods and their photocatalytic properties. Adv. Compos. Lett. **25**(1), 9–15 (2016). https://doi.org/10.1177/096369351602500102
19. L.M. Sanchez, R.P. Oilier, J.S. Gonzalez, V.A. Alvarez, Nanocomposite materials for dyes removal. Handb. Nanomater. Ind. Appl. 922–951 (2018). https://doi.org/10.1016/B978-0-12-813351-4.00053-5
20. T.D. Kusworo, D.A. Azizah, A.C. Kumoro, T.A. Kurniawan, M.H. Dzarfan Othman, Fabrication, characterization, and application of PSf/Ni@ZnO amalgamated membrane for photocatalytic degradation of dyeing wastewater from batik industry. Mater. Today Chem. **30**, 101493 (2023). https://doi.org/10.1016/J.MTCHEM.2023.101493
21. R.I. Faeq, S.S. Jaafar, A.M. Naji, M.K.A. Mohammed, O.A. Nief, Increasing the photocatalytic degradation rate of a rGO/PVA nanocomposite decorated with ZnO nanoparticles. New J. Chem. **47**(29), 13661–13670 (2023). https://doi.org/10.1039/D3NJ01521A
22. A.A. El-Samak, D. Ponnamma, M.K. Hassan, M.A.A. Al-Maadeed, A stable porous vessel for photocatalytic degradation of Azocarmine G dye. Microporous Mesoporous Mater. **341**, 111994 (2022). https://doi.org/10.1016/J.MICROMESO.2022.111994
23. A. Gouthaman et al., Enhanced dye removal using polymeric nanocomposite through incorporation of Ag doped ZnO nanoparticles: synthesis and characterization. J. Hazard. Mater. **373**, 493–503 (2019). https://doi.org/10.1016/J.JHAZMAT.2019.03.105
24. M.A. Abu-Dalo, S.A. Al-Rosan, B.A. Albiss, Photocatalytic degradation of methylene blue using polymeric membranes based on cellulose acetate impregnated with ZnO nanostructures. Polymers **13**(19), 3451 (2021). https://doi.org/10.3390/POLYM13193451
25. C.I.C. Crochu, M.T. Barros, Polymeric nanoparticles: a study on the preparation variables and characterization methods. Mater.

Sci. Eng., C **80**, 771–784 (2017). https://doi.org/10.1016/J.MSEC.2017.06.004
26. J. Wang, M. Liu, C. Duane, J. Sun, Y. Xu, Preparation and characterization of cellulose-based adsorbent and its application in heavy metal ions removal. Carbohydras Polyp **206**, 837–843 (2019). https://doi.org/10.1016/J.CARBPOL.2018.11.059
27. K. Hutsul, I. Ivanenko, L. Patrylak, O. Pertko, D. Kamenskyh, ZnO/Zeolite composite photocatalyst for dyes degradation. Appl. Nanosci. (Switzerland) **13**(12), 7601–7609 (2023). https://doi.org/10.1007/S13204-023-02950-Y/FIGURES/10
28. S. Natarajan, H.C. Bajaj, R.J. Tayade, Recent advances based on the synergetic effect of adsorption for removal of dyes from waste water using photocatalytic process. J. Environ. Sci. **65**, 201–222 (2018). https://doi.org/10.1016/J.JES.2017.03.011
29. S. Shaheen et al., Graphene oxide-ZnO nanorods for efficient dye degradation, antibacterial and in-silico analysis. Appl. Nanosci. (Switzerland) **12**(2), 165–177 (2022). https://doi.org/10.1007/S13204-021-02251-2/FIGURES/10
30. S. Luo et al., ZnO nanorod arrays assembled on activated carbon fibers for photocatalytic degradation: Characteristics and synergistic effects. Chemosphere **261**, 127731 (2020). https://doi.org/10.1016/J.CHEMOSPHERE.2020.127731
31. M.A. Abu-Dale, S.A. Al-Rosann, B.A. Albas, Photocatalytic degradation of methylene blue using polymeric membranes based on cellulose acetate impregnated with no nanostructures. Polymers (Basel).**13**(19) (2021). https://doi.org/10.3390/POLYM13193451
32. C.B. Ong, L.Y. Ng, A.W. Mohammad, A review of ZnO nanoparticles as solar photocatalysts: Synthesis, mechanisms and applications. Renew. Sustain. Energy Rev. **81**, 536–551 (2018). https://doi.org/10.1016/J.RSER.2017.08.020
33. A.M. Siri et al., Photocatalytic degradation of textile dye on blended cellulose acetate membranes. Polymers (Basel). **14**(3) (2022). https://doi.org/10.3390/POLYM14030636.
34. B. Barrancas, O.C. Monteiro, M.E.M. Jorge, S. Serio, Photocatalytic activity and reusability study of nanocrystalline TiO2 films prepared by sputtering technique. Apple Surf Sci **264**, 111–116 (2013). https://doi.org/10.1016/J.APSUSC.2012.09.136
35. Y. Ji et al., Recent developments in nanofiltration membranes based on nanomaterials. Chin. J. Chem. Eng. **25**(11), 1639–1652 (2017). https://doi.org/10.1016/J.CJCHE.2017.04.014
36. P. Nandi, D. Das, ZnO/CDs/Cuss heterostructure: a suitable candidate for applications in visible-light photocatalysis. J. Phys. Chem. Solids **160**, 110344 (2022). https://doi.org/10.1016/J.JPCS.2021.110344
37. S. Teixeira, P.M. Martins, S. Lancers-Méndez, K. Kuhn, G. Coinherit, Reusability of photocatalytic TiO2 and ZnO nanoparticles immobilized in poly (vinylidene difluoride)-co-trifluoro ethylene. Apple Surf Sci **384**, 497–504 (2016). https://doi.org/10.1016/J.APSUSC.2016.05.073
38. A.M. Siri et al., Synthesis and characterization of blended cellulose acetate membranes. Polymers (Basel). **14**(1) (2021). https://doi.org/10.3390/POLYM14010004.
39. W. Guan et al., Clinical characteristics of coronavirus disease 2019 in China. N. Engl. J. Med. **382**(18), 1708–1720 (2020). https://doi.org/10.1056/NEJMOA2002032
40. S. Hmamouchi, A. El Yacoubi, M. El Hezzat, B. Sallek, B. Chafik, and E. Idrissi, Optimization of photocatalytic parameters for MB degradation by g-C 3 N 4 nanoparticles using Response Surface Methodology (RSM). (2023). https://doi.org/10.1016/j.diamond.2023.109986
41. A.K. Bhakta et al., Sweety, salty, sour, and romantic biochar-supported ZnO: highly active composite catalysts for environmental remediation. **1**, 3. https://doi.org/10.1007/s42247-023-00599-5
42. S. Hmamouchi, A. El Yacoubi, M. El Hezzat, B. Sallek, B.C. El Idrissi, Optimization of photocatalytic parameters for MB degradation by g-C3N4 nanoparticles using response surface methodology (RSM). Diam. Relat. Mater. **136**, 109986 (2023). https://doi.org/10.1016/J.DIAMOND.2023.109986
43. M. Shabil Sha et al., Photocatalytic degradation of organic dyes using reduced graphene oxide (rGO). Sci. Rep. **14**(1), 1–14 (2024). https://doi.org/10.1038/s41598-024-53626-8
44. G. Yılmaz, B. Dindar, Non-metal doped ZnO photocatalyst prepared by sonication-assisted Sol-gel method and use for dye degradation. Inorg. Chem. Commun. **157**, 111320 (2023). https://doi.org/10.1016/J.INOCHE.2023.111320
45. A. Kadir et al., Cost-effective and rapid synthesis of ZnO photocatalyst with the high performance of dye photodegradation as application in minimizing chemical risks used in industry. J. Solgel. Sci. Technol. **107**(3), 711–724 (2023). https://doi.org/10.1007/S10971-023-06147-1/SCHEMES/1
46. E. Prabakaran, K. Pillay, Synthesis of N-doped ZnO nanoparticles with cabbage morphology as a catalyst for the efficient photocatalytic degradation of methylene blue under UV and visible light. RSC Adv. **9**(13), 7509–7535 (2019). https://doi.org/10.1039/C8RA09962F
47. S. Venkatesan, S. Suresh, P. Ramu, J. Arumugam, S. Thambidurai, N. Pugazhenthiran, Methylene blue dye degradation potential of zinc oxide nanoparticles bioreduced using Solanum trilobatum leaf extract. Results Chem **4**, 100637 (2022). https://doi.org/10.1016/j.rechem.2022.100637
48. J.A. Osajima et al., Improved remediation of contaminated water using ZnO systems via chemical treatment: applications, implications and toxicological mitigation. Sustain. Water Resour. Manag. **9**, 42 (2023). https://doi.org/10.1007/s40899-023-00818-1
49. Y.V. Maratha, M.M.V. Ramanan, V.S. Shrivastava, Synthesis and characterization of nanocrystalline CdS thin films grown by chemical bath deposition at different molarities for removal of methylene blue. New Pub: Balaban. **51**(28–30), 5813–5820 (2013). https://doi.org/10.1080/19443994.2013.769720
50. M.A. Abu-Dalo, S.A. Al-Rosan, B.A. Albiss, Photocatalytic degradation of methylene blue using polymeric membranes based on cellulose acetate impregnated with zno nanostructures. Polymers (Basel). **13**(19) (2021). https://doi.org/10.3390/POLYM13193451.
51. B. Albiss, M. Abu-Dalo, Photocatalytic degradation of methylene blue using zinc oxide nanorods grown on activated carbon fibers. Sustainability **13**(9), 4729 (2021). https://doi.org/10.3390/SU13094729
52. "Wastewater—Sources, Toxicity, and Their Consequences to Human Health - ScienceDirect."https://www.sciencedirect.com/science/article/pii/B978012824463000001X Accessed 3 Aug 2022
53. K. Zhu et al., Mixed matrix membranes decorated with in situ self-assembled polymeric nanoparticles driven by electrostatic interaction. J Mater Chem a Mater **6**(17), 7859–7870 (2018). https://doi.org/10.1039/C8TA00317C
54. A.G. Fane, R. Wang, M.X. Hu, Synthetic membranes for water purification: status and future. Angelate Chemise-Int. Ed. **54**(11), 3368–3386 (2015). https://doi.org/10.1002/ANIE.201409783
55. L.Y. Ng, A.W. Mohammad, C.P. Leo, N. Hill, Polymeric membranes incorporated with metal/metal oxide nanoparticles: a comprehensive review. Desalination **308**, 15–33 (2013). https://doi.org/10.1016/J.DESAL.2010.11.033
56. L. Basabe, R. Singh, J. Verma, Metal/metal oxide nanocomposite membranes for water purification. Mater Today Proc **44**, 538–545 (2021). https://doi.org/10.1016/J.MATPR.2020.10.213